Effects of CW Interference on Phase-Locked Loop Performance

Murat F. Karşı, *Member, IEEE,* and William C. Lindsey, *Fellow, IEEE*

***Abstract*—This paper focuses on the modeling and analysis of phase-locked loops in the presence of continuous wave (CW) interference such that the operating vulnerability to CW jamming and interference can be accessed. The loop phase error is characterized, and the conditions under which the loop remains locked in frequency to the desired carrier are presented. Analysis is conducted for arbitrary offsets of carrier and interferer signal frequencies relative to the quiescent voltage-controlled oscillator (VCO) frequency. The results show that loop performance depends not only on the frequency difference between the desired signal and interferer, but also on the frequency offset between the quiescent VCO oscillation and desired carrier. The vulnerability of the loop to the presence of interference increases if interferer and desired signal spectral locations are in opposite sides of quiescent VCO frequency.**

***Index Terms*—Interference, phase-locked loops, phase synchronization.**

I. Introduction

SYNCHRONIZATION of the local oscillator with the incoming carrier phase is fundamental to the demodulation process in a coherent communications receiver. In many circumstances, carrier synchronization system performance is degraded by both additive noise and interference. Due to crowding of the useful frequency spectrum, many systems are now being affected by interference more than they were a few decades ago. Interference signals may also be jamming signals from unfriendly sources or spurious signals generated in local oscillators.

In coherent communications systems that use a sinusoidal carrier and a phase-locked loop (PLL) to track the carrier phase such as deep space network, interference effects have proved to be important [1], [2]. Earth stations employed for space exploration are often operated in an environment of man-made electromagnetic radiation. Carrier synchronization is fundamental to telemetry and range-doppler measurements of DSN, and these are affected by interference [1]. So, interference effects are of importance for such systems because they can severely degrade synchronization and overall system performance.

Paper approved by M. Luise, the Editor for Synchronization of the IEEE Communications Society. This work was supported in part by LinCom Corporation. This paper was presented in part at MILCOM'94, Fort Monmouth, NJ, October 2–4, 1994.

M. F. Karşı was with the University of Southern California, Los Angeles, CA 90089 USA. He is now with IBM–Encinitas, Encinitas, CA 92024 USA (e-mail: murat@cts.com).

W. C. Lindsey is with LinCom Corporation, Los Angeles, CA 90056 USA. He is also with the University of Southern California, Los Angeles, CA 90089 USA.

Publisher Item Identifier S 0090-6778(00)04006-X.

An area of application where tracking a sinusoidal signal in the presence of interference is radar detection and tracking. For example, monopulse angle tracking radars are widely used for tracking airborne vehicles in which the receivers often use PLL's for coherent detection of the received signals [3]–[5]. In such systems, additional targets within the mainlobe of the radar antenna lead to additional sinusoidal signatures. Some systems operate on the output of an ordinary bandpass filter that is used instead of a PLL. In such systems, when there are multiple targets flying in close formation, the "temporal power centroid" of the two targets, which can be neither of them, will be tracked [3]. On the other hand, PLL trackers resolve and lock onto one of the incoming signals. A drawback of using PLL's is that the system may "jump" to track the secondary target when secondary target signal level exceeds a certain threshold, or if the secondary target signal frequency is very close to primary target signal frequency [4], [5].

The majority of studies on performance of carrier synchronization systems in the presence of interference assume the absence of noise affecting the system. If the signal-to-noise ratio (SNR) is so high that the primary agent affecting the system is the interferer, deterministic approach gives accurate results about system behavior. Analytical studies of [2]–[5], [8], [11], and [12] utilize harmonic balance method to analyze the dynamics of the phase error signal in the absence of noise. The conditions under which the loop stays locked to the desired carrier are derived for the specific case of no initial detuning between the desired carrier and the quiescent voltage-controlled oscillator (VCO) frequencies. Harmonic balance method will also be utilized in this paper and will be explained in detail in the next section. Another technique that has been utilized is the computer simulation by implementing the loop equation in a computer code and observing the phase error [6], [10].

A relatively small number of papers on synchronization system performance in the presence of both noise and interferers have been published [13]–[18]. One technique that has been used is the experimental observation of the system [13], [14]. In [15], numerical techniques are utilized for performance evaluation of second-order PLL in a noisy, specular plus diffuse multipath environment, and the standard deviation of the phase jitter is used as a criterion to yield performance curves. Computer simulation analysis in the presence and noise and interference are conducted in [16]. In [17] and [18], the joint effects of interference and additive noise on the PLL performance is analyzed with analytical methods. In [17], phase-error probability density function (pdf), its moments, and cycle slip statistics are evaluated for a first-order loop in the face of a single continuous wave (CW) interferer when

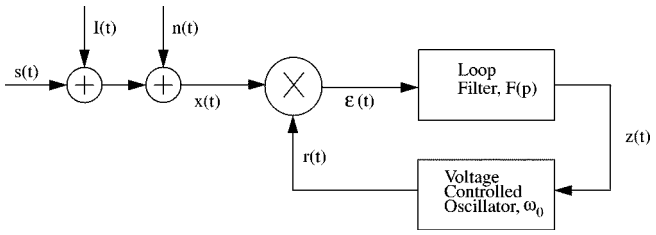

Fig. 1. PLL system block diagram.

there is no frequency offset between interferer and desired signal frequencies. In [18], an analysis for the special case of no frequency offset between the desired signal and quiescent VCO frequency is conducted by employing a different method.

In Section II, the carrier synchronization system model and the stochastic differential equation that governs the phase-error process are given.

In Section III, previous studies are generalized to analyze effects of arbitrary initial detuning between the quiescent VCO and desired signal frequencies. It is assumed that a single CW interferer exposes the system and noise is absent. The analysis with the assumption of absence of noise gives useful results for high SNR conditions. Phase error is characterized while the loop is locked to the desired signal, and the condition for the loop to remain locked in frequency to desired signal is derived.

In Section IV, a model that manifests the time evolution of the phase-error process in the presence of both additive noise and interference is developed. This model facilitates an extension of the previously available results to the case of arbirary frequency difference between the desired and interferer signals and arbitrary initial detuning between the quiescent VCO and desired signal frequencies. In the steady state, the phase-error process is modeled as sum of a periodic component and a stationary random process. By using this model, a Fokker–Planck analysis is conducted in order to obtain statistical insight into loop performance.

II. Carrier Synchronization System Model

Consider the PLL system block diagram given in Fig. 1. The system is exposed to an interference signal $I(t)$ in addition to desired signal $s(t)$ and noise $n(t)$.

Let the desired carrier, interference, and the VCO output signals be represented as

$$s(t) = \sqrt{2S}\,\sin\Phi(t) = \sqrt{2S}\sin(\omega_0 t + \theta(t)) = \sqrt{2S}\sin(\omega_0 t + \Omega_0 t + \theta_0) \tag{1}$$

$$I(t) = \sqrt{2J}\sin\Phi_i(t) = \sqrt{2J}\sin(\omega_0 t + \Omega_s t + \theta_s) \tag{2}$$

$$r(t) = \sqrt{2}\cos\hat{\Phi}(t) = \sqrt{2}\cos(\omega_0 t + \hat{\theta}(t)). \tag{3}$$

Here, the desired carrier signal $s(t)$ is assumed be of constant amplitude $\sqrt{2S}$ and of constant frequency and phase offsets (Ω_0 and θ_0) relative to the quiescent VCO oscillation (frequency ω_0). Similarly, the interference signal is of constant amplitude of $\sqrt{2J}$ and is of constant frequency and phase offsets Ω_s and θ_s relative to the quiescent VCO frequency and phase. The additive white Gaussian noise $n(t)$ is assumed to be a stationary process with zero mean and two-sided spectral density of height $N_0/2$ W/Hz.

With $s(t), r(t)$, and $I(t)$ as defined in (1)–(3), the equation that governs the loop phase error ($\varphi(t) \triangleq \Phi(t) - \hat{\Phi}(t)$) can be shown to satisfy [19]

$$\frac{1}{K\sqrt{S}}\frac{d\varphi(t)}{dt} = \gamma - F(p)\left[\sin\varphi(t) + \sqrt{R_s}\sin(\varphi(t) + \Delta\Omega t + \Delta\theta) + \frac{1}{\sqrt{S}}N(t)\right] \tag{4}$$

with

$$\gamma \triangleq \frac{\Omega_o}{K\sqrt{S}}, \qquad R_s \triangleq \frac{J}{S}. \tag{5}$$

Here, R_s is the interference power to the signal power ratio, K is the open loop gain, $\Delta\Omega \triangleq \Omega_s - \Omega_0$ and $\Delta\theta \triangleq \theta_s - \theta_0$ are the frequency and phase offsets between the interferer and the desired carrier, respectively, and $F(p)$ is the loop filter characterized in Heaviside operator notation ($p \triangleq (d/dt)$ is the Heaviside operator). For a first-order loop, the loop filter is identified by $F(p) = 1$, for a perfect second-order loop $F(p) = (1+pT_2)/pT_1$, and for an imperfect second-order loop $F(p) = (1+pT_2)/(1+pT_1)$. The noise process $N(t)$ in (4) is a stationary, white Gaussian noise zero mean and two-sided spectral density of height $N_0/2$ W/Hz [19].

We now introduce a few parameters for later use. Let $M(\omega) = |F(\omega)|$ and $P(\omega) = \angle(F(\omega))$ be the magnitude and phase response characteristics of the loop filter $F(\omega)$, respectively. The single-sided loop bandwidth obtained from linearized PLL theory B_L is given by $B_L = K\sqrt{S}/4$ for a first-order loop and $B_L = (r+1)/(4T_2)$ with $r \triangleq F_0 T_2 K\sqrt{S}$ and $F_0 = T_2/T_1$ for a second-order loop.

III. Loop Performance in the Absence of Additive Noise

Our goal is to characterize the phase-error process which is governed by (4), with $N(t) = 0$. We will use approximations in order to characterize the phase error in the region of interest of the signal and system parameters.

The force term in (4) (with $N(t) = 0$) is periodic in time due to presence of the CW interference. As a result, the phase error in steady state is periodic, and it can be represented in a cosine series. The nature of the phase trajectory and the number of significant harmonics in the solution varies significantly depending on the frequency offset between the interferer and the desired carrier, $\Delta\Omega$, relative to the linearized loop bandwidth B_L. As a result, the analysis can be dissected into the following three cases:

Case I: $|\Delta\Omega| \gg B_L$;
Case II: $|\Delta\Omega| \ll B_L$;
Case III: $|\Delta\Omega| \approx B_L$.

In most applications, Case I is of practical interest since typically the loop is designed to be narrow in order to track the incoming carrier with minimum phase error. As will be done in this paper, Cases I and II can be studied analytically. However, analytical treatment of Case III is intractable, and numerical solutions are necessary.

A. Case I: $|\Delta\Omega| \gg B_L$

Using the constant and first harmonic terms in the cosine series representation of phase error leads to the following model [2], [8], [9]:

$$\varphi(t) = c_0 + c_1 \cos(\Delta\Omega t + \Delta\theta + \psi_1). \tag{6}$$

The validity of this model is substantiated over a large range of desired carrier, interference and loop parameters and is also supported by experimental observation [9] and computer simulations of the authors. For determining $\varphi(t)$, one can insert (6) into (4) and use the "harmonic balance method" to obtain c_0, c_1, and ψ_1. The method involves, as the name implies, equating the relevant coefficients of each harmonic term of the left-hand side (LHS) and the right-hand side (RHS). Efforts to incorporate higher order harmonics in the harmonic balance method leads to untractable sets of equations.

Application of the method with the model given in (6) leads to

$$0 = \gamma - M(0)[J_0(c_1)\sin c_0 + \sqrt{R_s}J_1(c_1)\cos(c_0 - \psi_1)] \tag{7}$$

$$c_1 D\cos P(\Delta\Omega) = M(\Delta\Omega)\sqrt{R_s}[J_0(c_1)+J_2(c_1)]\cos(c_0-\psi_1) \tag{8}$$

$$\begin{aligned} c_1 D\sin P(\Delta\Omega) = M(\Delta\Omega)\{&\sqrt{R_s}[J_2(c_1) - J_0(c_1)] \\ &\times \sin(c_0 - \psi_1) - 2J_1(c_1)\cos c_0\}. \end{aligned} \tag{9}$$

Here, $D \triangleq \Delta\Omega/K\sqrt{S}$ is the detuning between the desired carrier and interference normalized by the loop gain, $J_0(\cdot), J_1(\cdot)$, and $J_2(\cdot)$ are Bessel functions of orders 0, 1, and 2, respectively. From (9), one can get two solutions for ψ_1 as

$$\begin{aligned} \psi_{1,1} &= c_0 - A \\ \psi_{1,2} &= c_0 + A - \pi \end{aligned} \tag{10}$$

where

$$A = \sin^{-1}\left\{\frac{1}{\sqrt{R_s}[J_2(c_1) - J_0(c_1)]} \cdot \left[\frac{c_1 D\sin P(\Delta\Omega)}{M(\Delta\Omega)} + 2J_1(c_1)\cos c_0\right]\right\}. \tag{11}$$

Here, $\sin^{-1}(\cdot)$ is defined in $[-\pi/2, \pi/2]$. The loop and system parameters determine which solution of ψ_1 will be valid for satisfying (7)–(9). For the range of parameters of interest (small c_1), it can be seen from (8) that $\psi_{1,1}$ is valid when $D > 0$ and $\psi_{1,2}$ is valid when $D < 0$ (Note that for the loop filters considered $\cos(P(\Delta\Omega)) > 0$).

Inserting (10) into (8), using the identity $J_2(x) = (2/x)J_1(x) - J_0(x)$, and rearranging the resulting equation yields

$$R_s = \left[\frac{c_1^2 D\cos P(\Delta\Omega)}{2M(\Delta\Omega)J_1(c_1)}\right]^2 + 4\left[\frac{\frac{c_1 D\sin P(\Delta\Omega)}{2M(\Delta\Omega)} + J_1(c_1)\cos c_0}{J_0(c_1) - J_2(c_1)}\right]^2. \tag{12}$$

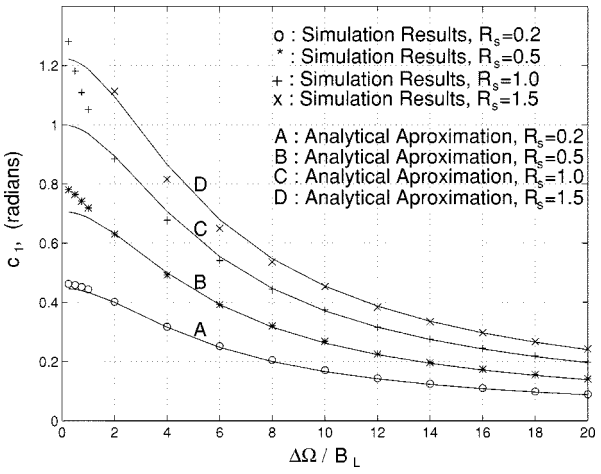

Fig. 2. Comparison of c_1 obtained from analytical approximations [from (15)] and by computer simulations for first-order loop ($R_s = 0.2, 0.5, 1.0, 1.5, \gamma = 0.0$).

Extracting $\cos(c_0 - \psi_1)$ from (8), inserting into (7), and rearranging the equation leads to

$$\sin c_0 = \left[\frac{\gamma}{M(0)} - \frac{c_1^2 D}{2}\frac{\cos P(\Delta\Omega)}{M(\Delta\Omega)}\right]\frac{1}{J_0(c_1)}. \tag{13}$$

1) Phase-Error Characteristics While the Loop Is Locked: Exact and explicit simultaneous solution of (10), (12), and (13) is impossible and it is necessary to utilize some approximations to get c_0, c_1, and ψ_1. Using $J_0(c_1) \approx 1, J_1(c_1) \approx c_1/2$, and $J_2(c_1) \approx 0$ (accurate for $c_1 < 1$) in (12) yields

$$c_1^2 = \frac{R_s}{D^2\left[\left(\frac{\cos P(\Delta\Omega)}{M(\Delta\Omega)}\right)^2 + \left(\frac{\sin P(\Delta\Omega)}{M(\Delta\Omega)} + \frac{\cos c_0}{D}\right)^2\right]}. \tag{14}$$

Utilizing the unperturbed value of $c_0 = \sin^{-1}\gamma$ in the absence of interference in (12) to yield an approximation for c_1, and using $J_0(c_1) \approx 1$ in (13) leads to

$$c_1^2 = \frac{R_s}{D^2\left[\left(\frac{\cos P(\Delta\Omega)}{M(\Delta\Omega)}\right)^2 + \left(\frac{\sin P(\Delta\Omega)}{M(\Delta\Omega)} + \frac{\sqrt{1-\gamma^2}}{D}\right)^2\right]} \tag{15}$$

$$\sin c_0 = \frac{\gamma}{M(0)} - \frac{{c_1}^2 D}{2}\frac{\cos P(\Delta\Omega)}{M(\Delta\Omega)}. \tag{16}$$

The value of ψ_1 can be obtained by using c_1 and c_0 obtained from (15) and (16) in (10). Above results reduce to earlier results for the special case of $\gamma = 0$ [9].

In Fig. 2, we have plotted c_1 versus $\Delta\Omega/B_L$ for first-order loop for $R_s = 0.2, 0.5, 1.0$, and 1.5. For $R_s = 1.5$, the simulation results for small $\Delta\Omega/B_L$ are missing The loop loses its frequency lock to the desired carrier in this range. For a given value of $\Delta\Omega/B_L$, as R_s increases, c_1 increases. In the range $\Delta\Omega/B_L > 2$, the analytical approximations are close to simulation results. In the range $\Delta\Omega/B_L < 2$, the analytical approximations are close to simulation results for small R_s. As

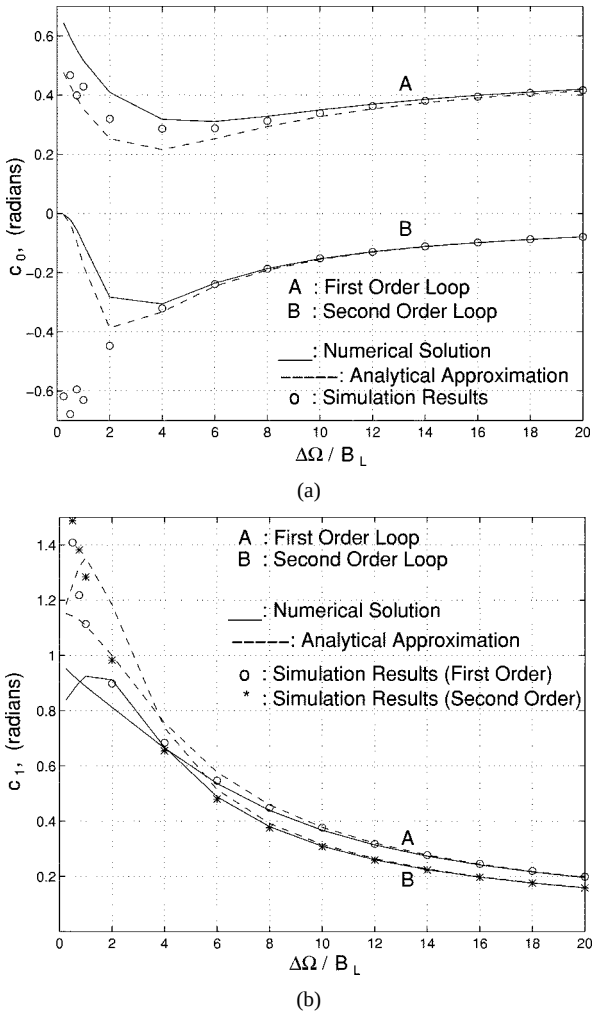

Fig. 3. Comparison of (a) c_0 and (b) c_1 obtained from analytical approximations [from (16)], by numerical solution of (7)–(9) and by computer simulations for first and perfect second-order loops ($R_s = 1, \gamma = 0.5$, for second-order loop, $F_0 \triangleq T_2/T_1 = 0.025, r = 4$).

R_s gets larger, the analytical results start deviating from simulation results. This is due to two reasons. First, as R_s gets large, in the range $\Delta\Omega/B_L < 2, c_1$ gets so large that the assumption of $c_1 < 1$ that leads to simplified expressions does not hold. Second, the nature of the steady-state phase trajectory is not satifactorily represented with the first harmonic in the cosine series expansion of the phase error. This can be seen through the following arguement. For $R_s = 0.5$, the analytical approximation results deviate from simulation results in the range $\Delta\Omega/B_L < 2$. We have $c_1 \approx 0.75$ in this range. For $R_s = 1.0$ and $R_s = 1.5$, $c_1 = 0.75$ is reached at larger values of $\Delta\Omega/B_L$. However, the analytical approximation results are close to simulation results for $c_1 \approx 0.75$ on the curves for $R_s = 1.0$ and $R_s = 1.5$. Similarly for the case of $R_s = 1$, the analytical approximation results deviate from simulation results in the range $\Delta\Omega/B_L < 2$. We have $c_1 \approx 1.1$ in this range. From the curve $R_s = 1.5$, the analytical approximation is close to simulation results for $c_1 = 1.1$.

In Fig. 3, we present comparison of c_0 and c_1 obtained from (15) and (16), obtained by numerical solution of (7)–(9) and from computer simulations conducted by software implementation of the loop equation (4) (with $N(t) = 0$) as a function of $\Delta\Omega/B_L$ for $R_s = 1$. The results are given for first and perfect second-order loops. For readability of the curves, the results for imperfect second-order loop which are very close to the curves of perfect loop are not given. Note that the accuracy of (15) and (16) increases as c_1 decreases. Since c_1 decreases with decreasing R_s and with increasing $\Delta\Omega$, the accuracy of the approximations improves as R_s decreases and $\Delta\Omega$ increases.

2) The Conditions for Losing Frequency Lock in the Absence of Additive Noise: If the loop is locked in frequency to the desired carrier, the average instantaneous frequency of the VCO should equal the desired signal frequency and the phase-error evolution is periodic. Thus, for anytime t_0, the phase error should satisfy the following relation:

$$\int_{t_0}^{t_0+(2\pi/|\Delta\Omega|)} \dot{\varphi}(t)\,dt = \varphi\left(t_0 + \frac{2\pi}{|\Delta\Omega|}\right) - \varphi(t_0) = 0. \quad (17)$$

If the loop is not locked in frequency to the desired carrier, the average frequency of the VCO output differs from the frequency of the desired carrier, thus, the phase error is no longer periodic and it is not possible to satisfy (17). Thus, (17) gives a frequency-lock criterion for the loop. Since (7) is obtained by integration of (4) (with $N(t) = 0$) over the time interval of $2\pi/|\Delta\Omega|$ with $\varphi(t)$ given in (6), it has the same meaning as (17) in terms of loop and interference parameters. Then, in order to obtain the conditions that ensure lock to the desired carrier, one should find the conditions under which it is possible to establish (7). Starting from (7) to (9), we had reached (15) and (16). Examination of (15) reveals that as R_s is increased, c_1 increases. In (16) (which is a rearranged form of (7) after the approximations are introduced), if c_1 increases, the RHS increases or decreases (depending on the sign of $\Delta\Omega$) without bound. At a certain critical value of c_1, the RHS exceeds one in magnitude and it is no longer possible to solve (16). We denote this value of c_1 as $c_{1,\mathrm{cr}}$ and the value of R_s that leads to $c_{1,\mathrm{cr}}$ as $R_{s,\mathrm{cr}}$. Clearly, if $R_s < R_{s,\mathrm{cr}}$, (16) [thus (15)] and (7) can be established and there is a stable lock point. On the other hand, if R_s is increased beyond $R_{s,\mathrm{cr}}$, a stable lock point does not exist and the loop cannot stay locked in frequency to the desired signal. In order to get $c_{1,\mathrm{cr}}$ and $R_{s,\mathrm{cr}}$, we set $\sin c_0$ to -1 or $+1$ accordingly with the sign of $\Delta\Omega$. From (16), we get

$$c_{1,\mathrm{cr}}^2 = \left(\frac{\gamma}{M(0)} + \mathrm{sgn}(\Delta\Omega)\right)\frac{2}{D}\frac{M(\Delta\Omega)}{\cos P(\Delta\Omega)}. \quad (18)$$

If we also set $\cos c_0 = 0$ in (14), it follows that $c_{1,\mathrm{cr}} = \sqrt{R_{s,\mathrm{cr}}}M(\Delta\Omega)/|D|$. Thus

$$R_{s,\mathrm{cr}} = \left(\frac{\gamma}{M(0)} + \mathrm{sgn}(\Delta\Omega)\right)\frac{2D}{M(\Delta\Omega)\cos P(\Delta\Omega)}. \quad (19)$$

These results reduce to earlier results of [2] and [9] for $\gamma = 0$.

In order to display the vulnerability of the loop types considered so far, we display $R_{s,\mathrm{cr}}$ versus $\Delta\Omega/B_L$ for first, perfect second-order, and imperfect second-order loops in Fig. 4 for $\gamma = 0.0$ and $\gamma = 0.5$. The first-order loop is inferior to second-order loops with respect to holding its frequency lock to the desired carrier. For $\gamma = 0$, the perfect and the imperfect loops act similarly. It is observed that the performance of the

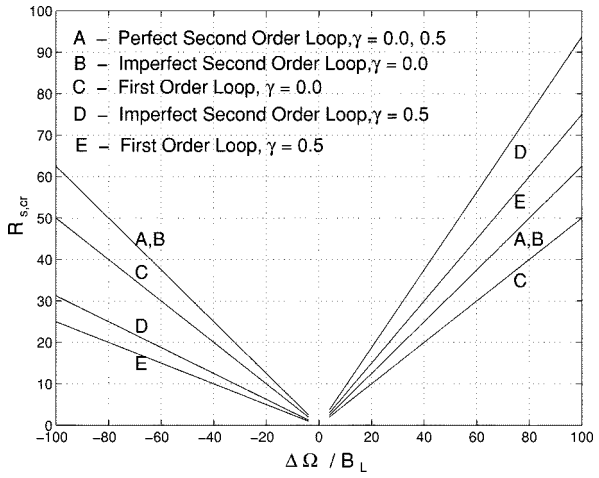

Fig. 4. $R_{s,\mathrm{cr}}$ versus $\Delta\Omega/B_L$ for first, perfect, and imperfect second-order Loops ($\gamma = 0.0, 0.5$, for second-order loops $F_0 \triangleq T_2/T_1 = 0.025$, $r = 4$).

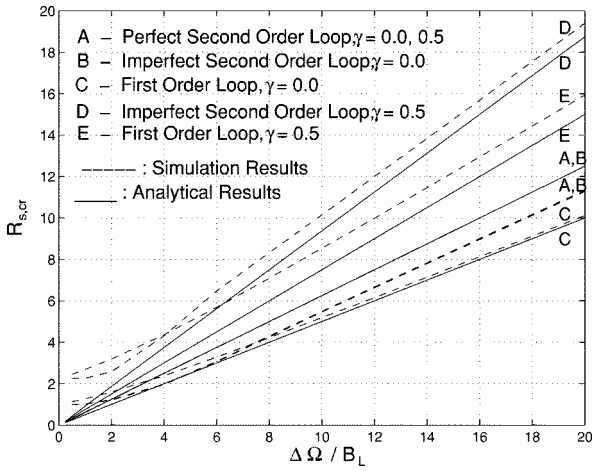

Fig. 5. Comparison of analytical and simulation results $R_{s,\mathrm{cr}}$ versus $\Delta\Omega/B_L$ for first, perfect, and imperfect second-order loops ($\gamma = 0.0, 0.5$, for second-order loops, $F_0 \triangleq T_2/T_1 = 0.025$, $r = 4$).

perfect second-order loop is not affected by initial detuning in the loop. This can also be seen by examination of (18) and (19) by observing the presence of the loop filter pole at origin for a perfect loop ($M(0) = \infty$). However, imperfect second-order loop and the first-order loop are highly vulnerable to initial detuning. For example, for $\gamma = 0.5$, the loop is more vulnerable to CW effects for negative values of $\Delta\Omega$ rather than positive values of $\Delta\Omega$.

This leads to the following idea for improving PLL performance against CW interference for first and imperfect second-order loops. If difference Ω_0 is measured and a control signal is applied to the VCO so that the quiescent frequency of the VCO is the same as the desired carrier frequency, effectively Ω_0 is set to zero, and the system will not suffer from the above quoted effect when an interferer of arbitrary frequency is introduced. Measurement of the difference between quiescent VCO frequency and the desired carrier frequency may be conducted by observing the dc level shift at the input of the VCO when the desired carrier is introduced. The control of quiescent VCO oscillation frequency can be performed by applying an offset voltage at the VCO input.

In Fig. 5, a comparison of analytical results obtained from (19) and computer simulation results for a first-order loop is presented. Simulations are conducted by implementing the loop equation in a digital computer and observing the phase-error trajectory. It is shown that the results obtained through the approximations give results that are close to simulation results for large $\Delta\Omega/B_L$.

In Fig. 5, we see that in the range $\Delta\Omega/B_L < 4$, the analytical approximation for $R_{s,\mathrm{cr}}$ [as given by (19)] does not follow the simulation results closely. The reasons for this are as follows. First, as $\Delta\Omega$ becomes smaller, as implied by approximate analysis, $c_{1,\mathrm{cr}}$ becomes larger. However, the main assumption we used for reaching simplified analytical results was $c_1 < 1$. Thus, the approximations are no longer valid. Another reason that contributes to the invalidity of the approximations for $\Delta\Omega < B_L$ is that (6) is no longer an accurate model for the phase-error signal, and higher harmonic contents of $\varphi(t)$ are significant. As a result, the simple models given in (14) and (16) are not sufficient to describe loop behavior for this case. Thus, for assuring the validity of (19) over the range of R_s under which the loop stays locked in frequency to the desired signal, it should be assumed that $\Delta\Omega \gg B_L$. This condition was used in [8] for the analysis to be tractable.

B. Case II: $|\Delta\Omega| \ll B_L$

For analysis of the loop when $|\Delta\Omega| \ll B_L$, an alternative method is required. In this case, the period of beatnotes of $\varphi(t)$, $T_b \triangleq 2\pi/|\Delta\Omega|$, is much larger than the loop time constants, and it is possible to analyze the PLL behavior with a completely different method. The loop time constants are in the order of $1/B_L$. With the $|\Delta\Omega| \ll B_L$ assumption, T_b is much bigger than the loop time constants, and the the loop can converge to a steady-state regime while the time-varying force term in (4) remains relatively constant. Then, one can use the instantaneous value of $\Delta\Omega t + \Delta\theta \triangleq \Delta\theta'$ as a constant for short-term analysis of the loop. Note that due to mismatch between the desired carrier and the interfering frequency, $\Delta\theta'$ is a function of time.

By using simple trigonometric identities, it is possible to write (4) (with $N(t) = 0$) as

$$\frac{1}{K\sqrt{S}}\frac{d\varphi(t,\Delta\theta')}{dt} = \gamma - F(p)\sqrt{1+R_s+2\sqrt{R_s}\cos\Delta\theta'} \cdot \sin\left[\varphi(t) + \tan^{-1}\left(\frac{\sqrt{R_s}\sin\Delta\theta'}{1+\sqrt{R_s}\cos\Delta\theta'}\right)\right]. \tag{20}$$

If the loop phase error converges to a stable lock point while $\Delta\theta'$ is constant, the LHS of (20) is zero and $\varphi(t,\Delta\theta')$ is a constant. Let us denote the steady-state value of $\varphi(t,\Delta\theta')$ as $\varphi_{\mathrm{ss}}(\Delta\theta')$. From (20), we have

$$\varphi_{\mathrm{ss}}(\Delta\theta') = \sin^{-1}\left[\frac{\gamma/F(0)}{\sqrt{1+R_s+2\sqrt{R_s}\cos(\Delta\theta')}}\right] - \tan^{-1}\left[\frac{\sqrt{R_s}\sin(\Delta\theta')}{1+\sqrt{R_s}\cos(\Delta\theta')}\right] \pm 2n\pi. \tag{21}$$

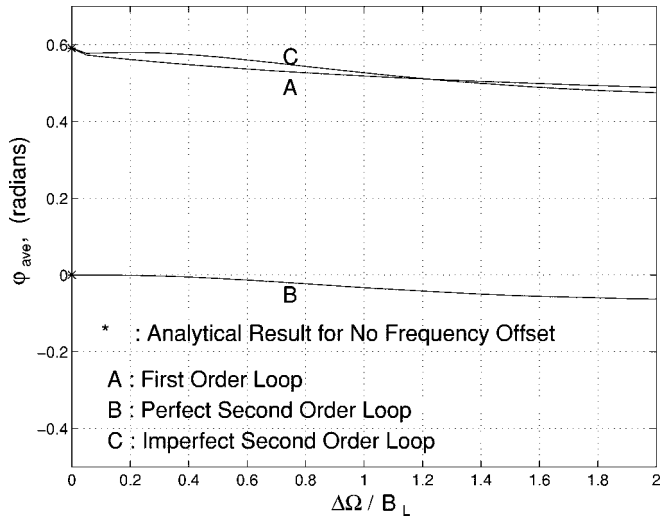

(a)

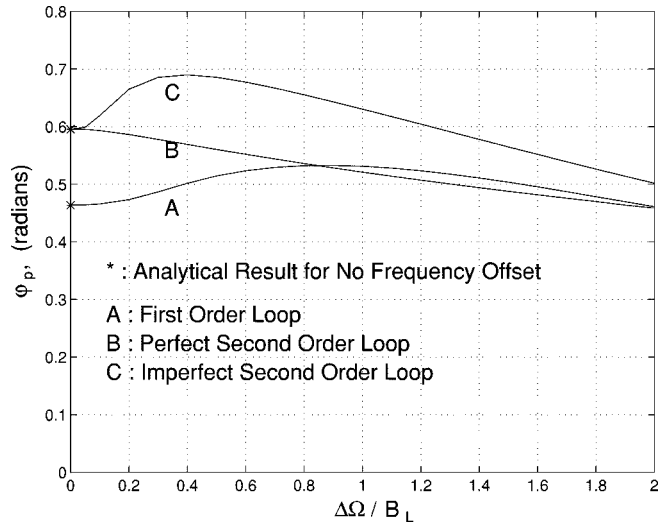

(b)

Fig. 6. Simulation results for (a) the average $\varphi_{\rm ave}$ and (b) the oscillation magnitude φ_p of the phase error $\varphi(t)$ versus $\Delta\Omega/B_L$ and the approximation for $\Delta\Omega = 0$. ($R_s = 0.2, \gamma = 0.5$. For second-order loop, $F_0 \triangleq T_2/T_1 = 0.025, r = 4.0$).

Here, n is any integer and $\sin^{-1}(\cdot)$ is defined in $[-\pi/2, \pi/2]$. For imperfect second-order and first-order loops $F(0) = 1$. For a perfect second-order loop, $F(0) = \infty$, and the first term in (21) vanishes (except for the case of R_s and $\Delta\theta' = \pi$, for which the interference cancels the desired signal and loop operation is not possible).

We are interested in seeing the extent to which characterization of $\varphi(t)$ obtained by varying $\Delta\theta'$ in $\varphi_{\rm ss}(\Delta\theta')$ continues to hold when $\Delta\Omega/B_L \neq 0$. We have conducted computer simulations and measured the average $\varphi_{\rm ave}$ and the magnitude φ_p of the phase-error oscillations for various values of $\Delta\Omega/B_L$ in the interval $0 < \Delta\Omega/B_L < 2$. We define oscillation magnitude as half of peak-to-peak variation of the phase error. In Fig. 6, we plot the average $\varphi_{\rm ave}$ and oscillation magnitude φ_p of the phase error as a function of $\Delta\Omega/B_L$ in the interval $0 < \Delta\Omega/B_L < 2$. In this figure, the results obtained by finding the average and half of peak-to-peak variation of $\varphi(t)$ from (21), with $\Delta\theta'$ varying in $[0, 2\pi]$ are given at $\Delta\Omega/B_L = 0$. It is shown that the phase-error characteristics (average value and peak-to-peak variations) do not change in a drastic manner drastically as $\Delta\Omega/B_L$ changes in the interval $[0, 2]$.

The approximation given (21) can be used to access loop vulnerability to a CW interferer which is within the loop bandwidth. We will give the condition under which the loop equation (20) has a stable solution. This will give the conditions that quarantee that the loop will continue to stay frequency locked as $\Delta\theta'$ varies in $[0, 2\pi]$. It is possible to reach (21) only if

$$-1 \leq \frac{\gamma/F(0)}{\sqrt{1 + R_s + 2\sqrt{R_s}\cos(\Delta\theta')}} \leq 1. \tag{22}$$

Since $\Delta\theta' \epsilon [0, 2\pi]$ and the smallest value of the denominator in (22) is $|1 - \sqrt{R_s}|$ (it is attained when $\Delta\theta' = \pi$), in order for (20) to have a stable solution for arbitrary $\Delta\theta'$, one should have

$$\left| \frac{\gamma/F(0)}{1 - \sqrt{R_s}} \right| \leq 1. \tag{23}$$

Equation (23) is actually a condition for the loop to hold its frequency lock to the desired signal in the absence of noise. If (23) is satisfied, there is a stable solution for (20), and, thus, there is a stable operating point for the loop. If (23) is not satisfied, (20) does not have a stable solution. For the case of $R_s = 1$, with $\Delta\theta = \pi$ the interference cancels the desired signal, signal presence is lost, and the loop cannot track the desired signal. For a perfect second-order loop, (23) is always satisfied, since $F(0) = \infty$ (except for $R_s = 1$, for which with $\Delta\theta' = \pi$, the interference cancels the desired signal, and loop operation is not possible). For imperfect second- and first-order loops, the range of R_s values with which there is a stable operating point can be explicity written as (from (23) with $F(0) = 1$)

$$R_s \leq (1 - |\gamma|)^2 \tag{24}$$

$$R_s \geq (1 + |\gamma|)^2. \tag{25}$$

IV. Loop Performance in the Presence of Additive Noise

In the presence of noise, the problem has to be dissected with respect to relative magnitudes of $|\Delta\Omega|$ and B_L in the same manner as was done in the analysis with the assumption of absence of noise. For case I ($|\Delta\Omega| \gg B_L$), we present an analysis that uses suitable approximations to obtain the Fokker–Planck equations that govern the phase-error statistics. For the case of $|\Delta\Omega| \approx B_L$ numerical solutions for the time-independent Fokker–Planck equation corresponding to (4) is necessary. In this paper, we do not attempt to present such solutions. If $|\Delta\Omega| \ll B_L$, the period of the beatnote in (4) is much larger than the loop time constants. Similar to the idea of the analysis we conducted in the absence of interference, one may conduct a short-term analysis of the loop while assuming that the the interferer is at the same frequency with the desired signal and phase of the interferer is constant. In [17], statistics for the phase-error process for this case has been derived. When the interferer is not exactly of same frequency, as a worst-case analysis, performance parameters of interest can be obtained through averaging over the phase of the interfering signal.

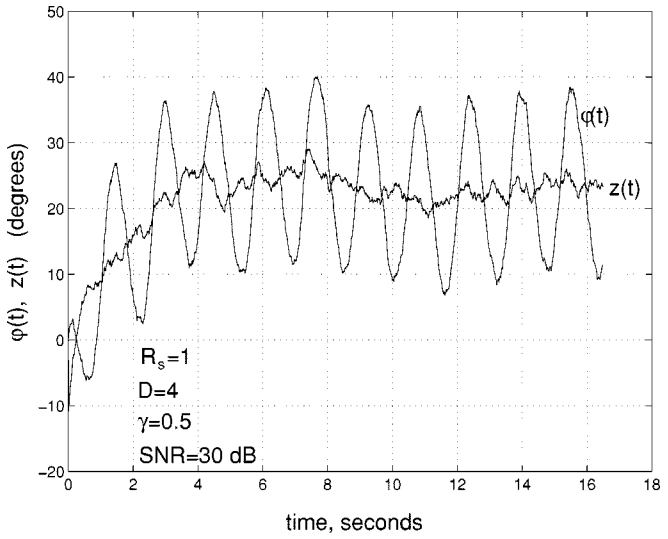

Fig. 7. $\tilde{z}(t)$ and $\varphi(t)$ for a typical operation scenario for a first-order PLL ($\gamma = 0.5, D = 4, R = 1, K = 1, S = 1$, and $\mathrm{SNR} \triangleq \rho = 30$ dB).

A. Approximate Model Development for Phase-Error Evolution

We develop an approximate model for the evolution of the phase-error process by utilizing a technique which is similar to the Krylov–Boguliubov method for analysis of underdamped sinusoidal oscillators [20], [21].

In the absence of noise, when $|\Delta\Omega| \gg B_L$ the phase error was satisfactorily modeled to be of the form given in (6). We assume the following form for the evolution of the phase-error process:

$$\varphi(t) = \tilde{z}(t) + c_1 \cos(\psi_1 + \Delta\Omega t + \Delta\theta). \tag{26}$$

Here, $\tilde{z}(t)$ is a random process whose statistics will be determined through the following analysis. The second term in (26) is a periodic sinusoidal term whose parameters are determined by the earlier analysis in absence of noise of this paper. In the absence of noise, $\tilde{z}(t) = c_0$. In the presence of noise we assume that $\tilde{z}(t)$ is slowly varying relative to $T_b \triangleq 2\pi/|\Delta\Omega|$. As an illustration, in Fig. 7, we give trajectories of $\varphi(t)$ and $\tilde{z}(t)$ of (26) for a first-order loop for a specific choice of loop and signal parameters.

Differentiating (26) with respect to time and inserting $\dot{\varphi}(t)$ from (4), we get the stochastic differential equation for time evolution of $\tilde{z}(t)$

$$\begin{aligned}\frac{1}{K\sqrt{S}}\dot{\tilde{z}}(t) = \gamma - F(p)\Big[&\sin(\tilde{z}(t) + c_1\cos(\psi_1 + \Delta\Omega t + \Delta\theta)) \\ &+ \sqrt{R_s}\sin(\tilde{z}(t) + c_1\cos(\psi_1 + \Delta\Omega t + \Delta\theta) \\ &+ \Delta\Omega t + \Delta\theta) + \frac{1}{\sqrt{S}}N(t)\Big] \\ &+ c_1 D\sin(\psi_1 + \Delta\Omega t + \Delta\theta).\end{aligned} \tag{27}$$

With the second term on the RHS of (26), we characterize the deterministic time variations of $\varphi(t)$. For the parameter range of interest, we assume that the periodic variations of $\tilde{z}(t)$ caused by the periodic forcing due to presence of interference is negligible. In (27), the force terms are periodic with T_b on the RHS, and one can use the average these terms of (27) over T_b to get the dynamic behavior of $\tilde{z}(t)$. This has the same meaning as approximating the first and second terms inside the brackets and the last term on the RHS of (27) by their average values. The resulting equation of evolution can be obtained in a straightforward manner as

$$\begin{aligned}\frac{1}{K\sqrt{S}}\dot{\tilde{z}} = \gamma - F(p)\Big[&(J_0(c_1) + \sqrt{R_s}J_1(c_1)\sin\psi_1)\sin\tilde{z} \\ &+ \sqrt{R_s}J_1(c_1)\cos\psi_1\cos\tilde{z} + \frac{1}{\sqrt{S}}N(t)\Big].\end{aligned} \tag{28}$$

Equation (28) is a stochastic differential equation with time-independent coefficients. Thus, it can be analyzed by standard Fokker–Planck techniques.

We will call $\tilde{z}(t)$ the **time-averaged phase-error process** since its dynamics is described by the stochastic differential equation whose force term is obtained by averaging the time-varying force term of the the stochastic differential equation describing the phase-error process $\varphi(t)$. It should be noted that $\tilde{z}(t)$ is of unbounded variance as time increases. The phase error disperses along the "$\tilde{z}$" axis as time increases, and its variance becomes infinite. As is customary in analysis of phase tracking systems in the presence of noise whose equation of operation is a stochastic differential equation of the form (28), we shall work with modulo-2π reduced version of $\tilde{z}(t)$ which we call $z(t)$. Thus, in what follows, the Fokker–Planck equation describing the statistics of $z(t)$ will be solved with 2π periodic boundary conditions in "z". Let

$$\phi(t) \triangleq z(t) + c_1\cos(\psi_1 + \Delta\Omega t + \Delta\theta). \tag{29}$$

From (29), the instantaneous pdf of $\phi(t)$ conditioned on $t, \Delta\Omega$, and $\Delta\theta$ is

$$p(\phi, t, \Delta\theta, \Delta\Omega) = p_z(\phi - c_1\cos(\psi_1 + \Delta\Omega t + \Delta\theta), \Delta\Omega) \tag{30}$$

where $p_z(z, \Delta\Omega)$ is the pdf of $z(t)$ conditioned on $\Delta\Omega$. Note that the statistics of $z(t)$ does not depend on $\Delta\theta$ [see (28)]. For $p_z(z, \Delta\Omega)$, we use the subscript "z" contary to the notation in the rest of the paper to signify that the density considered is that of the variable "z". In the steady state, the mean of $\phi(t)$ conditioned on $t, \Delta\Omega$, and $\Delta\theta$ ($\triangleq m(\phi, t, \Delta\theta, \Delta\Omega)$) can be written as

$$\begin{aligned}m(\phi, t, \Delta\theta, \Delta\Omega) &\triangleq \overline{\phi(t)} \\ &= \overline{z(t)} + c_1\cos(\psi_1 + \Delta\Omega t + \Delta\theta) \\ &= m(z, \Delta\Omega) + c_1\cos(\psi_1 + \Delta\Omega t + \Delta\theta)\end{aligned} \tag{31}$$

where overbar denotes statistical expectation over noise and $m(z, \Delta\Omega)$ is the mean of $z(t)$. Note that $m(z, \Delta\Omega)$ is independent of time. Using (29), the conditional mean square value $\overline{\phi^2(t)}$ of the phase-error process can be calculated as

$$\begin{aligned}\overline{\phi^2(t)} = \overline{z^2(t)} &+ 2\overline{z(t)}c_1\cos(\psi_1 + \Delta\Omega t + \Delta\theta) \\ &+ c_1^2\cos^2(\psi_1 + \Delta\Omega t + \Delta\theta).\end{aligned} \tag{32}$$

From (31) and (32), it follows that variance of the phase error is $\sigma^2(\phi, t, \Delta\theta, \Delta\Omega) = \sigma^2(z, \Delta\Omega)$, where $\sigma^2(z, \Delta\Omega)$ is the variance of $z(t)$.

B. PDF of the Time-Averaged Phase-Error Process

Equation (28) can be writen in the following form:

$$\frac{1}{K\sqrt{S}}\dot{\tilde{z}} = \gamma - F(p)\left[M_0\sin(\tilde{z}+P_0) + \frac{1}{\sqrt{S}}N(t)\right] \quad (33)$$

where

$$M_0 \triangleq \sqrt{A_1^2+A_2^2} \quad P_0 \triangleq \tan^{-1}(A_2/A_1) \quad (34)$$

$$A_1 \triangleq [J_0(c_1) + \sqrt{R_s}J_1(c_1)\sin\psi_1] \quad (35)$$

$$A_2 \triangleq \sqrt{R_s}J_1(c_1)\cos\psi_1. \quad (36)$$

Equations of the type (33) has been studied extensively in [19]. In particular, (28) represents the equation of operation of a second-order tracking loop with phase detector characteristics $g(z) = M_0\sin(z+P_0)$.

Results of [19] can be utilized to yield the steady-state pdf $p(z)$ of the modulo-2π reduced process $z(t)$ for the second-order loop

$$p(z,\Delta\Omega) = \frac{1}{4\pi^2 e^{-\beta_1\pi}|I_{j\beta_1}(\alpha_1)|^2}e^{\beta_1 z+\alpha_1\cos(z+P_0)} \cdot\int_z^{z+2\pi} e^{-[\beta_1 y+\alpha_1\cos(y+P_0)]}\,dy. \quad (37)$$

where

$$\beta_1 = \left(\frac{rM_0+1}{rM_0}\right)\frac{\rho' M_0^2}{F_0}\left[\frac{\gamma}{M_0} - (1-F_0)\overline{\sin(z+P_0)}\right] \times\left[1+\frac{F_0}{\rho' M_0^2(rM_0+1)\sigma_G^2}\right] \quad (38)$$

$$\alpha_1 = \left(\frac{rM_0+1}{rM_0}\right)\rho' M_0^2 - \frac{1}{rM_0\sigma_G^2} \quad (39)$$

$$F_0 \triangleq \frac{T_2}{T_1}, \qquad r \triangleq F_0 T_2 K\sqrt{S} \quad (40)$$

$$\rho' \triangleq \frac{S}{N_0 B_L'}, \qquad B_L' = \frac{rM_0+1}{4T_2}. \quad (41)$$

$$\sigma_G^2 \triangleq \overline{\sin^2(z(t)+P_0)} - \overline{\sin(z(t)+P_0)}^2. \quad (42)$$

Here, $I_{j\beta_1}(\cdot)$ is the Bessel function of imaginary order $j\beta_1$. The pdf for a first-order loop $(F(p)=1)$ is given by (37) with parameter definitions $\alpha_1 = M_0\alpha$, where $\alpha = (4\sqrt{S}/N_0K)$ and $\beta_1 = \gamma\alpha$. In the absence of interference, the pdf for a first-order loop $(F(p)=1)$ is given by (37) with $P_0 = 0, \alpha_1 = \alpha$, and $\beta_1 = \beta = \gamma\alpha$. Here, we introduced the parameter β to denote the value of β_1 in the absence of interference.

From (33), by comparison with the pdf in the absence of interferer $(R_s = 0, M_0 = 1, P_0 = 0)$, one can recognize the fact that the effect of the interfering tone is to introduce a bias, P_0 to $z(t)$, and modify the effective input signal level to the loop by a factor of M_0.

In Fig. 8, $p(z,\Delta\Omega)$ for several interference scenarios for first and second-order loops are given. For being able to present numerical results, it is necessary to assume particular approximations to c_1, c_0, and ψ_1. In the figures in the rest of this study, we employ (10), (15), and (16) for approximation of c_1, c_0, and ψ_1. In both figures, we choose the SNR in the loop bandwidth ($\triangleq\rho$) to be 6 dB. In terms of loop parameters, we have $\rho \triangleq S/(N_0B_L)$. For a first-order loop, $\rho = \alpha$.

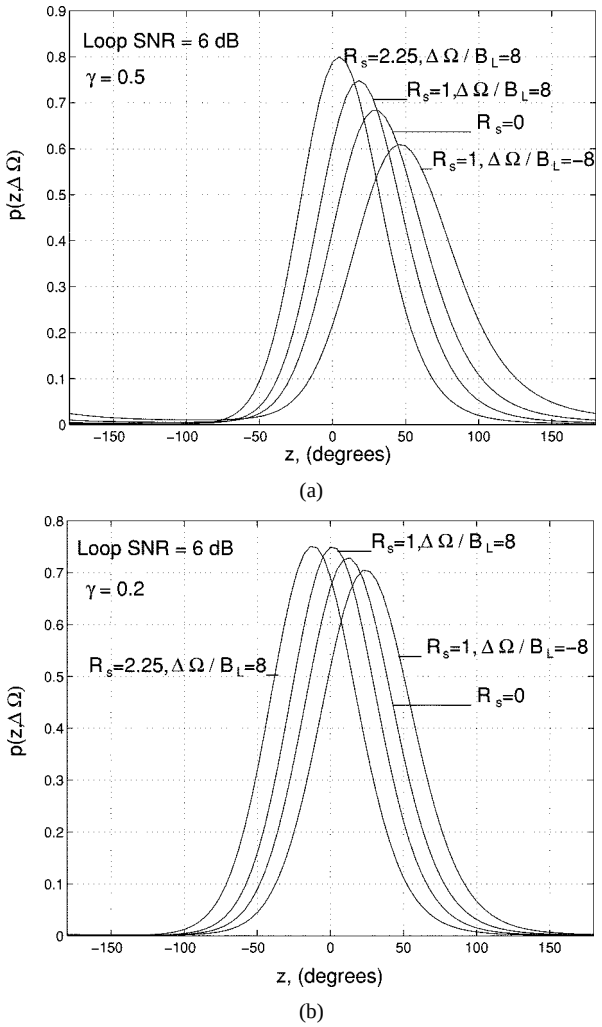

Fig. 8. Steady-state pdf of time-averaged phase-error process $z(t)$ for various interference scenarios for (a) first-order and (b) second-order loops. For first-order loop, $\rho = 4, \gamma = 0.5$, for second-order loop, $F_0 = 0.002, r = 4, \rho = 4, \gamma = 0.2$.

In Fig. 9, $p(z,\Delta\Omega)$ obtained through (37) and by computer experiments for a first-order loop for two different interference scenarios are compared. The computer simulations are conducted by direct implementation of (4) on a digital computer. The phase-error trajectories that are obtained by running the codes several times are used to extract the parameters of the model given in (26). It is shown that (26) is a suitable model for the phase error. It should be noted that the approximate solutions given in (10), (15), and (16) are most accurate for $c_1 < 1$. For $R = 5, c_1$ is not much smaller than unity and the approximation for $p(z,\Delta\Omega)$ does not exactly follow the simulation results. A more detailed account of the simulation procedure and extensive results pertaining to comparison of analytical and simulation results can be found in [16].

In Fig. 10, the mean $m(z,\Delta\Omega)$ of the time-averaged phase-error process as a function of interference to desired carrier magnitude ratio R_s is depicted for several values of $\Delta\Omega/B_L$ for first

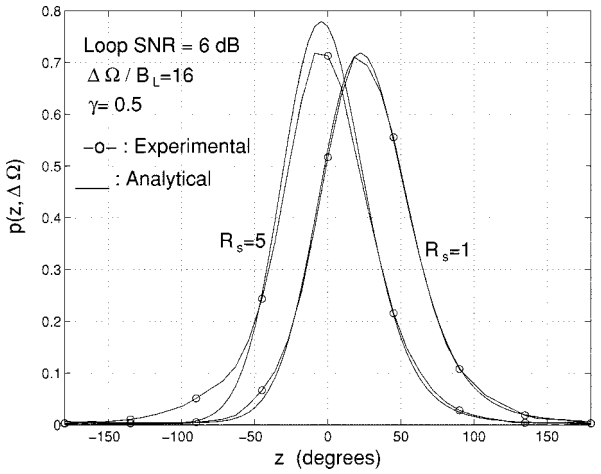

Fig. 9. Comparison of analytical results with computer simulations for first-order loop. ($\rho = 4, \gamma = 0.5$).

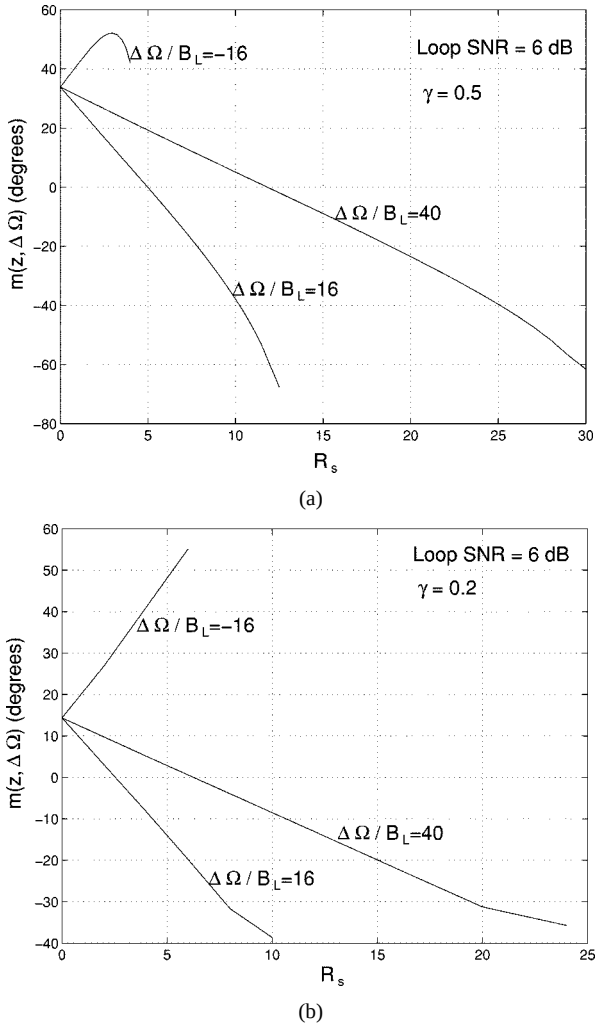

Fig. 10. Mean $\sigma(z, \Delta\Omega)$ versus R_s for various values of $\Delta\Omega/B_L$ for (a) first-order loop and (b) second-order loop. For first-order loop, $\rho = 4, \gamma = 0.5$, and for second-order loop, $F_0 = 0.002, r = 4, \rho = 4, \gamma = 0.2$.

and second-order loops. Similarly, plots for standard deviation $\sigma(z, \Delta\Omega)$ for first and second-order loops are given in Fig. 11.

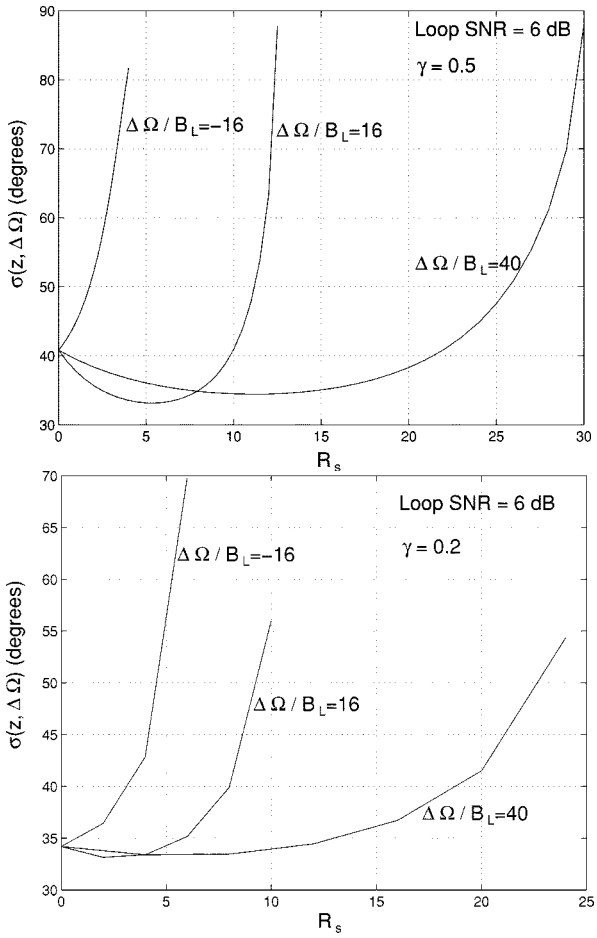

Fig. 11. Standard deviation $\sigma(z, \Delta\Omega)$ versus R_s for various values of $\Delta\Omega/B_L$ for (a) first-order loop and (b) second-order loop. For first-order loop, $\rho = 4, \gamma = 0.5$, and for second-order loop, $F_0 = 0.002, r = 4, \rho = 4, \gamma = 0.2$.

In the figures, some portions of the graphs may seem to be incomplete. The noiseless analysis of the loop reveals that at these portions the frequency lock to the desired carrier is lost.

C. Statistical Dynamics of the Time-Averaged Phase-Error Rate in a First-Order Loop

From (28), since $N(t)$ is a zero-mean noise process and $\sin\tilde{z} = \sin z$ and $\cos\tilde{z} = \cos z$, we can formally write the mean rate for $\tilde{z}(t)$ as ([19])

$$\dot{\bar{\tilde{z}}} = \dot{\bar{z}} = K\sqrt{S}\int_{-\pi}^{\pi}[\gamma - (J_0(c_1) + \sqrt{R_s}J_1(c_1)\sin\psi_1)\sin z - (\sqrt{R_s}J_1(c_1)\cos\psi_1)\cos z]p(z)\,dz. \quad (43)$$

Here, overbar denotes statistical expectation. Note that $\dot{\bar{z}} = 2\pi[N_z^+ - N_z^-]$ where N_z^+ and N_z^- are the average number of cycle slips in the positive and negative "z" directions per time unit.

By using standard techniques [19] from (37) and (43), it is straightforward to show that

$$N_z^+ - N_z^- = \frac{\Omega_0}{2\pi}\frac{\operatorname{sinch}(\beta_1\pi)}{|I_{j\beta_1}(\alpha_1)|^2}. \quad (44)$$

Here, $\mathrm{sinch}(x) \triangleq \sinh(x)/x$. For any given "$z$," the ratio of positive and negative cycles slip rates is given by [19]

$$\frac{N_z^+}{N_z^-} = e^{[U(z)-U(z+2\pi)]} = e^{2\pi\beta_1}. \tag{45}$$

From (45) and (44), the individual slip rates in the positive and negative directions can be determined as

$$N_z^{\pm} = K\sqrt{S}\frac{1}{4\pi^2\alpha}\frac{e^{\pm\pi\beta_1}}{|I_{j\beta_1}(\alpha_1)|^2}. \tag{46}$$

Then, the total number of cycle slips in the positive and negative directions per unit time is

$$T_z \triangleq N_z^+ + N_z^- = K\sqrt{S}\frac{1}{2\alpha}\frac{\cosh(\pi\beta_1)}{\pi^2|I_{j\beta_1}(\alpha_1)|^2}. \tag{47}$$

D. Statistical Dynamics of the Phase-Error Rate in a First-Order Loop

For given $\Delta\theta$ and $\Delta\Omega$, from (29)

$$\begin{aligned}\bar{\dot{\phi}}(t) &= \overline{\dot{z}(t)} - c_1\Delta\Omega\sin(\psi_1 + \Delta\Omega t + \Delta\theta) \\ &= \bar{\dot{z}} - c_1\Delta\Omega\sin(\psi_1 + \Delta\Omega t + \Delta\theta).\end{aligned} \tag{48}$$

Thus, in the steady state, $\bar{\dot{\phi}}(t)$ is a periodic function of time. We will further average $\bar{\dot{\phi}}(t)$ over any interval of $2\pi/|\Delta\Omega|$, the period of the beatnote of the nonstationary phase-error process to yield the **time-averaged mean phase-error rate**

$$\bar{\dot{\phi}}_{\mathrm{ave}} \triangleq \frac{\Delta\Omega}{2\pi}\int_{t_0}^{t_0+(2\pi/|\Delta\Omega|)} \bar{\dot{\phi}}(t)\,dt. \tag{49}$$

The usage of time-averaged phase-error process for characterizing cycle slip behavior can easily be substantiated as follows. The basic assumption in deriving the model in (26) was that the time constants of the loop are larger compared to $2\pi/|\Delta\Omega|$. During typical operation of the loop, the expected time intervals between two consecutive cycle slips are much greater than the smallest the loop time constants. Thus, with respect to cycle slip behavior, the averaging formulated in (49) will not lead to any loss in performance evaluation.

It is immediately seen from (49) and (48) that $\bar{\dot{\phi}}_{\mathrm{ave}} = \bar{\dot{z}}$. Thus, the time-averaged mean phase-error rate is equal to the mean rate of time-averaged phase-error process. Hence, the dynamic behavior of $\phi(t)$ can be studied by studying the dynamic behavior of $z(t)$. The implication of this argument is that the net number of cycle slips of $\phi(t)$ is given by (44). Also, the results given in (45)–(47) apply directly in describing the cycle slip behavior of $\phi(t)$. Thus, we have $N_\phi^+ = N_z^+$ and $N_\phi^- = N_z^-$ where N_ϕ^+ and N_ϕ^- are the cycle slip rates.

Dynamic behavior of $\phi(t)$ is embedded in $z(t)$ in a time-averaged fashion. Thus, the above result is hardly surprising. In fact, if one examines the model of the evolution of the phase-error process given in (26), $c_1\cos(\psi_1 + \Delta\Omega t + \Delta\theta)$ term is just an additional oscillatory term. Thus, the above result was already implied by (26).

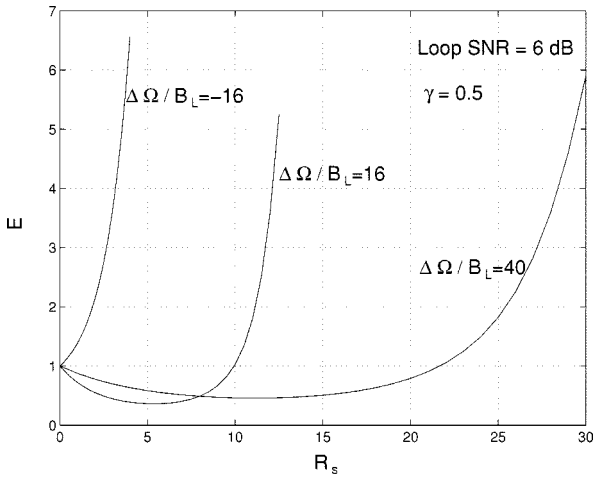

Fig. 12. Increase factor E versus R_s for various values of $\Delta\Omega/B_L$ for first-order loop ($\rho = 4, \gamma = 0.5$).

In the absence of interference, we name the cycle slip rates in positive and negative directions and the sum of cycle slip rates in positive and negative directions as N_a^+, N_a^-, and T_a. The effect of introduction of interference on the cycle slip rates can then be examined by the ratios

$$E \triangleq \frac{N_\phi^+}{N_a^+} = \frac{N_\phi^-}{N_a^-} = \frac{T_\phi}{T_a} = \frac{|I_{j\beta}(\alpha)|^2}{|I_{j\beta_1}(\alpha_1)|^2}. \tag{50}$$

Here, we made use of the fact that $M_0 = 1$ and $\beta_1 = \beta$ in the absence of interference. The term "E" denotes the increase factor in the slip rates by the introduction of the interference. In Fig. 12, this increase factor for various interference scenarios is presented.

V. Conclusion

The vulnerability of PLL's to CW interference is analytically characterized under suitable approximations. Previous studies are generalized to simultaneously take arbitrary initial frequency detuning between the desired signal and the quiescent VCO frequencies and arbitrary interferer frequencies into account. An approximate model for phase-error evolution in the presence of interference and additive noise is introduced, and its validity is verified with computer simulations.

The initial detuning between the desired carrier and the quiescent VCO frequencies has been found to be imperative on PLL performance in the presence of CW interference if the loop filter does not have a pole at origin. If there is initial detuning, first-order and imperfect second-order PLL performance depends on the frequency difference between the desired carrier and interference signals, not only in absolute value but also in sign.

Acknowledgment

The authors would like to thank one anonymous reviewer for his careful reading of the original version of the paper, particularly for his/her suggestions on how to reformulate the statistics of the phase-error process and how to use numerical methods to verify the region of validity of the approximate solutions.

REFERENCES

[1] M. K. Sue, "DSN RFI Susceptibility Model Development Program Overview," JPL, Pasadena, CA, Deep Space Network Prog. Rep. 42–68, Jan.–Feb. 1982.

[2] B. K. Levitt, "Carrier Tracking Loop Performance in the Presence of Strong CW Interference," JPL, Pasadena, CA, Deep Space Network Prog. Rep. 42–51, Mar.–Apr. 1979.

[3] I. E. Kliger and C. F. Olenberger, "Multiple target effects on monopulse signal processing," *IEEE Trans. Aerosp. Electron. Syst.*, vol. AES-11, pp. 795–804, Sept. 1975.

[4] ——, "Phase Locked Loop jump phenomenon the presence of two signals," *IEEE Trans. Aerosp. Electron. Syst.*, vol. AES-12, pp. 55–63, Jan. 1976.

[5] T. Endo and T. Suzuki, "Influence of an interfering target on a certain amplitude-comparison monopulse radar system," in *Proc. IEEE Global Telecommunications Conf.*, Atlanta, GA, Nov. 26–29, 1984, pp. 224–229.

[6] C. F. Olenberger, "Effects of automatic gain control on phase locked loop behavior in the presence of interference," *IEEE Trans. Aerosp. Electron. Syst.*, vol. AES-12, pp. 803–805, Nov. 1976.

[7] R. E. Ziemer, "Perturbation analysis of the effect of CW interference in Costas loop," in *Rec. National Telecommunications Conf.*, Houston, TX, Dec. 4–6, 1972, pp. 20-G1–20-G2.

[8] A. Blanchard, "Interferences in phase locked loops," *IEEE Trans. Aerosp. Electron. Syst.*, vol. AES-10, pp. 686–697, Sept. 1974.

[9] F. Bruno, "Tracking performance and loss of lock of a carrier loop due to the presence of a spoofed sperad spectrum signal," in *Proc. 1973 Symp. Spread Spectrum Communications*, vol. I, M. L. Schiff, Ed.. San Diego, CA, Mar. 13–16, 1973, pp. 71–75.

[10] A. Kantak and F. Davarian, "Performance of PLL in the presence of a CW interferer," in *Proc. IEEE Global Telecommunications Conf.*, Atlanta, GA, Nov. 26–29, 1984, pp. 230–236.

[11] N. K. Abdulaziz and S. D. Marougi, "Effect of an AGC amplifier on the performance of a generalized PLL in the presence of a large interfering signal," *Proc. Inst. Elect. Eng.*, pt. G, vol. 136, no. 4, pp. 178–183, Aug. 1983.

[12] M. F. Karşı and W. C. Lindsey, "Effects of CW interference on carrier tracking," in *Proc. MILCOM'94*, Ft. Monmouth, NJ, Oct. 2–5, 1994.

[13] R. E. Ziemer *et al.*, "RFI in hybrid loops—Simulation and experimental results," in *Rec. National Telecommunications Conf.*, Houston, TX, Dec. 4–6, 1972, pp. 32F-1–32F-6.

[14] C. L. Britt and D. F. Palmer, "Effects of CW interference on narrowband second order phase locked loops," *IEEE Trans. Aerosp. Electron. Syst.*, vol. AES-3, pp. 123–135, Jan. 1967.

[15] A. E. Smith *et al.*, "A digital simulation of of a carrier demodulator/tracking phase locked loop in a noisy multipath environment," in *EASCON '68 Rec.*, 1968, pp. 206–216.

[16] M. F. Karşı, "Effects of interferences on carrier synchronization," Ph.D. dissertation, Univ. of Southern California, May 1998.

[17] C. Y. Yoon and W. C. Lindsey, "Phase locked loop performance in the presence of CW interference and additive noise," *IEEE Trans. Commun.*, vol. COM-30, pp. 2305–2311, Oct. 1982.

[18] B. C. Sarkar, "Phase error dynamics of a first order phase locked loop in the presence of co-channel tone interference and additive noise," *IEEE Trans. Commun.*, vol. 38, pp. 962–965, July 1990.

[19] W. C. Lindsey, *Synchronization Systems in Communications and Control*. Englewood Cliffs, NJ: Prentice-Hall, 1982.

[20] M. Vidyasagar, *Nonlinear Sysytems Analysis*. Englewood Cliffs, NJ: Prentice-Hall, 1978.

[21] P. Jung, "Thermal activation in bistable systems under external periodic forces," *Z. Phys. B—Condensed Matter*, vol. 76, pp. 521–535, 1989.

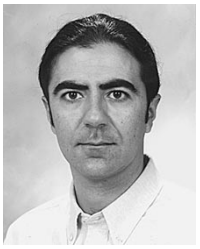

Murat F. Karşı (S'90–M'98) received the B.Sc. and M.Sc. degrees in electrical and electronic engineering from Middle East Technical University, Ankara, Turkey, *with honors*, in 1987 and 1989, respectively. He received the Ph.D. degree in electrical engineering from the University of Southern California, Los Angeles, in 1998.

In 1995, he joined CommQuest Technologies, Encinitas, CA, where he was responsible for system architecture, algorithm design, and performance analysis of second and third generation wireless communications transceivers. Since July 1998, he has been with IBM Microelectronics Division in Encinitas, CA, following the acquisition of CommQuest Technologies by IBM. His research interests include synchronization, A/D conversion, modulation, and signal processing for communications.

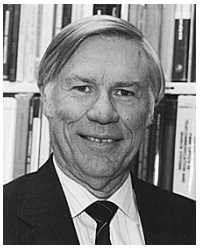

William C. Lindsey (S'61–M'63–SM'73–F'74) is Professor of Electrical Engineering at the University of Southern California, Los Angeles, CA, and serves as Chairman of the Board at LinCom Corporation, Los Angeles, CA, which he founded in 1974. He has been a frequent consultant to government and industry. He has published numerous papers on varied topics in communication theory and holds several patents. He has written three books: *Synchronization Systems in Communication and Control* (Englewood Cliffs, NJ: Prentice-Hall, 1972); *Telecommunication Systems Engineering*, co-authored with M. K. Simon (Englewood Cliffs, NJ: Prentice Hall, 1973; revised edition, Dover Publications, 1991); *Digital Communication Techniques: Signal Design and Detection*, co-authored with M. K. Simon and S. M. Hinedi (Englewood Cliffs, NJ: Prentice Hall, 1995). He is also co-author of *Phase-Locked Loops and Their Applications* (IEEE Press Book).

Dr. Lindsey is a member of the National Academy of Engineering (NAE). He serves on Commission C, Signals and Systems of the International Scientific Radio Union (URSI), and was Vice President of Technical Affairs of the IEEE Communications Society. He also served as the second Chairman of the Communication Society and is a former Editor of ComSoc. Currently, he serves as an editor for the Journal on Communications and Networks.